Hindawi
Mathematical Problems in Engineering
Volume 2018, Article ID 8474389, 13 pages
https://doi.org/10.1155/2018/8474389

Research Article

Experimental and Numerical Study on Hydrodynamic Performance of an Underwater Glider

Yanji Liu,[1,2] Jie Ma,[1,2] Ning Ma,[1,2] and Zhijian Huang[3]

[1]*State Key Laboratory of Ocean Engineering, Shanghai Jiao Tong University, Shanghai 200240, China*
[2]*School of Naval Architecture, Ocean and Civil Engineering, Shanghai Jiao Tong University, Shanghai 200240, China*
[3]*Merchant Marine College, Shanghai Maritime University, Shanghai 201306, China*

Correspondence should be addressed to Jie Ma; jma@sjtu.edu.cn

Received 6 February 2018; Revised 13 April 2018; Accepted 30 May 2018; Published 30 August 2018

Academic Editor: Muhammad N. Akram

The hydrodynamic coefficients are important parameters for predicting the motion of the glider and upgrading the hull design. In this paper, based on the Reynolds number similarity theory, 6 degrees of freedom (DOFs) of the fluid force and torque of a 1:1 full-scale glider model are measured. The present measurements were carried out at (2 – 14m/s) by varying attack angles and sideslip angles (-9 – 9°), respectively. The measurements were used to study the variation of the hydrodynamics of the glider, and the measurements have also been used to validate results obtained from a CFD code that uses RNG k – ε. The hydrodynamic force coefficients obtained from CFD accord well with the measurements. However, the torque coefficients difference is fairly large. Dynamics simulation results show that CFD results can be used to design and study the motion characteristics of gliders. In order to simplify the design process of gliders, we fit the empirical formula based on the experimental data and obtain a drag coefficient equation with Reynolds number. The influence of two kinds of appendages of the Conductance-Temperature-Depth (CTD) unit and thruster unit on the glider drag were studied by a contrast test. The analysis results can provide reference for design and the motion investigate of gliders.

1. Introduction

Underwater gliders have been widely applied to the environmental monitor for a large water area [1]. Underwater glider is a buoyance driven underwater vehicle. The mass and the buoyance are about the same and with a low gliding speed [2–4]. The hydrodynamic coefficients have a significant impact on gliders' designing and movement [5, 6].

The hydrodynamic coefficients of the streamlined hull can be obtained by numerical calculation. Underwater gliders are streamlined, the more accurate solution can be obtained by using a numerical method, such as a half-experience method [7], CFD [8], and strip theory [9]. However, there are some deviations between the numerical calculation and the measured results because the ideal model is used in the numerical calculation [10, 11]. The hydrodynamic parameters of underwater gliders can be obtained by a pool test [12]. However, the measurement process is rather complicated in towing tank. In addition to the tank test, the identification test and the wind tunnel test can obtain the hydrodynamic parameters. The identification method can obtain the fluid parameters based on the actual operating results. However, in the identification process, the vehicle is easy to be disturbed by the external environment, resulting in the deviation of the identification results [13]. The iterative process based on a large number of experimental data can improve the identification accuracy. However, collecting a large amount of experimental is rather difficult [14].

The steady hydrodynamic parameters can be obtained by means of a wind tunnel test based on the similarity theory. The test process is simple in the wind tunnel and the impacts of the free surface can be avoided on the measurement results. Berman [15] designed a 1:4.47 Slocum scale ratio model, measured the three-freedom-degree hydrodynamic parameters in the wind tunnel, and carried out the comparative analysis with theoretical calculation results. Techy et al. [16] tested

the six-freedom-degree steady hydrodynamic parameters of a 1:1 full-scale Seaglider in the wind tunnel and analyzed the impact of the CTD sensors on drag.

Movement path is important to gliders. Excellent path following ability is also an important destination of glider design and motion control. In this paper, based on mathematical model of the glider, the test results and numerical results are compared and analyzed, and the differences between the paths under the two groups of coefficients are analyzed, in order to illustrate the applicability of the results.

The 6-DOF dynamic equations of underwater gliders are nonlinear. The equations involve multiple variables. Thus it is difficult to obtain the global optimal solution. In this study, the particle swarm optimization (PSO) algorithm is used to obtain the solution. This algorithm is inspired by the social behavior of a bird flock. Through maintaining a population of candidate solutions, called particles, this algorithm is supposed to reach a global optimal solution.

The underwater glider has a streamlined hull with low drag. However, its plug-in sensors, propellers, and other accessories will influence its streamline and thus increase drag. It is difficult to accurately predict the magnitude of the drag produced by the CTD because the CTD complicated shape and installation position on the shell will have impacts on the drag [16, 17]. In this paper, the impacts of the streamlined CTD sensors on the fuselage drag are studied.

The underwater glider mainly glides in steady state and, with the increase of the performance for the glider, a propeller is usually installed at the end of the glider in order to improve the gliding speed [18, 19]. Unlike traditional AUV, the glider propeller only starts within a specified period of time and, while the propeller is not running, as an add-on static appendage, it will generate additional drag. To reduce the impact of the propeller on the fuselage hydrodynamic force, Chen et al. [20] designed a foldable propeller and revealed the impacts of different propeller angles on the hydrodynamic force. However, the foldable propellers are not commonly used at the present time. The propeller can be installed outside or inside the water deflector [21]. In this paper, the impacts of the add-on and built-in propellers on the fuselage drag in accordance with the test measurement results of the drag are studied and analyzed.

2. Experimental Programme

2.1. Experimental Setup. This study applies a 1:1 full-scale model of an underwater glider. The model has a pair of horizontal wings and a vertical tail wing, while the CTD sensor model is placed under the left horizontal wing. The test model hull and horizontal wings are made from carbon fiber; the head and tail water deflectors and the vertical tail wing are made from plastic. The model is 4.5 kg in total weight. See Figure 1 for the physical model and scale, with the main parameters being shown in Table 1.

To study the impacts of the CTD and the propeller on the hydrodynamic force of the glider, four kinds of test configurations have been adopted as shown in Table 2. See Figure 2 for installation forms of the two kinds of propellers in Configuration 3 and Configuration 4.

Table 1: Parameters of underwater glider.

Main scale	value
Total length (m)	2.350
Hull diameter (m)	0.216
Wing span (m)	1.318
Wings area (m^2)	0.165
Average chord length (m)	0.150
Model mass (kg)	4.200

Table 2: Test configurations.

Configuration	CTD	Propeller
Configuration 1	Present	Absent
Configuration 2	Absent	Absent
Configuration 3	Present	Built-in
Configuration 4	Present	Add-on

The test wind tunnel is 14m long, 6m wide, and 3.5m high, with a maximum wind speed up to 20m/s and with the velocity distribution precision$\leqslant \pm 0.8\%$. The measuring sensor adopts a six-component dynamic load balance SRI subject to a 16-bit sampling resolution with the force and torque measurement ranges of (-70 -70N) and (-70 -70N.m), respectively. The model to be tested is connected to the sensor by means of a 0.34-meter-long streamlined support bar located under the model center of gravity while the bar has its upper and lower pivots connected with the model and SRI separately. The sensor is fixed on a rotatable chassis.

The glider coordinate system is defined as shown in Figure 3, in which [X, Y, Z] indicate the force in three directions, [T1, T2, T3] indicate the torques around the three axles, and the directions follow the right-hand rule.

The hydrodynamic forces in wind coordinate are

$$F_A^w = \begin{bmatrix} -D \\ SF \\ -L \end{bmatrix} = R^{w/b} \begin{bmatrix} X \\ Y \\ Z \end{bmatrix}, \tag{1}$$

where $R^{w/b}$ is the transfer matrix from body coordinate to wind coordinate

$$R^{w/b} = \begin{bmatrix} \cos\alpha\cos\beta & \sin\beta & \sin\alpha\cos\beta \\ -\cos\alpha\sin\beta & \cos\beta & -\sin\alpha\sin\beta \\ -\sin\alpha & 0 & \cos\alpha \end{bmatrix}. \tag{2}$$

2.2. Experimental Procedure. The glider is subject to the conventional cruise speed of 0.25m/s and, during cruising, its attack angle and sideslip angle are generally kept within $\pm 5^\circ$ [17, 22]. In order to obtain the changing trend of the parameters more clearly, a larger angle is selected usually. In this test, the attack and sideslip angles are designed for testing change between ($-9 - 9^\circ$). The glider equipped with a propeller can achieve a higher velocity and due to which the hydrodynamic performance is more complex [19]. To test the performance of the glider at a high velocity, the movement

(a) Test model

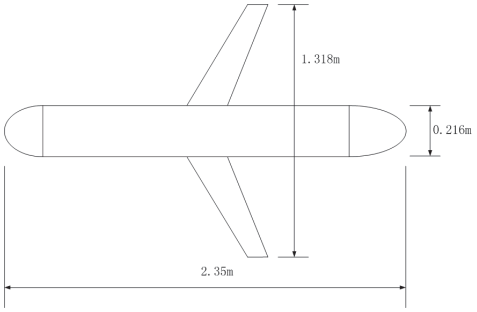

(b) Model scale top view

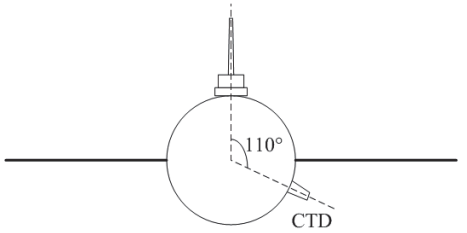

(c) Model scale front view

Figure 1: Test model of underwater glider.

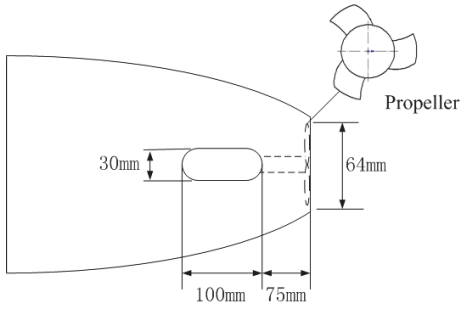

(a) Configuration 3

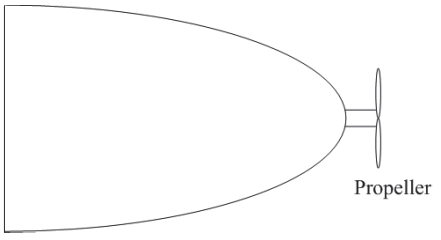

(b) Configuration 4

Figure 2: Propeller configuration.

Table 3: Parameters in wind tunnel.

Parameter definition	Description
Velocity (m/s)	0.15, 0.25, 0.35, 0.5, 0.6, 0.8, 1.0
Attack angle (˚)	-9, -6, -3, 0, 3, 6, 9
Sideslip angle (˚)	-9, -6, -3, 0, 3, 6, 9

speed in water designed for test changes between (0.15 – 1.0 m/s). See Table 3 for the settings of the test parameters.

Because the gliding velocity of glider is slow, usually in 0.5m/s, Reynolds number similarity criterion is used to convert velocity in different flow fields. The typical Reynolds number similarity criterion can be computed as follows:

$$\mathrm{Re} = \frac{\mathrm{V}l}{\gamma}, \tag{3}$$

where V is velocity of flow field, l is characteristic length, and γ is kinematic viscosity.

During testing, the temperature and humidity change within (19.7 – 23.3˚C) and (42 –57%), respectively. Select 15˚C fresh water as the operating environment and the corresponding kinematic viscosity is 1.1386×10^{-6} m^2/s. According to (3), the corresponding wind speed is about 2.0, 3.3, 4.6, 6.6,

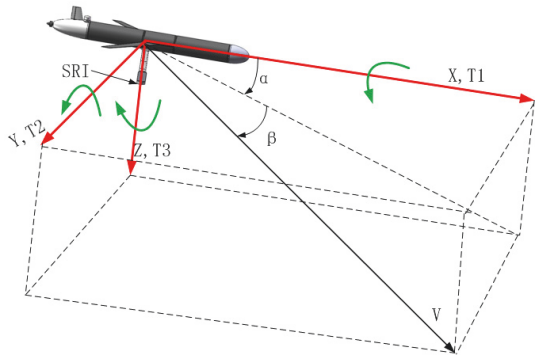

Figure 3: Underwater glider coordinate system.

8.0, 11.0, and 13.5 m/s, respectively, and the Reynolds numbers will change within $(3\times10^5-2\times10^6)$.

See (4) and (5) for the correspondence of the hydrodynamic force, torque, and coefficient.

$$\begin{aligned}
\text{Drag}\quad D &= \frac{1}{2}\rho C_D(\alpha)\,AV^2\\
\text{Lift}\quad L &= \frac{1}{2}\rho C_L(\alpha)\,AV^2 \qquad (4)\\
\text{Pitching moment}\quad T_2 &= \frac{1}{2}\rho C_{T_2}(\alpha)\,\bar{c}AV^2,
\end{aligned}$$

$$\begin{aligned}
\text{Sideforce}\quad SF &= \frac{1}{2}\rho C_{SF}(\beta)\,AV^2\\
\text{Rolling moment}\quad T_1 &= \frac{1}{2}\rho C_{T_1}(\beta)\,bAV^2 \qquad (5)\\
\text{Yawing moment}\quad T_3 &= \frac{1}{2}\rho C_{T_3}(\beta)\,bAV^2,
\end{aligned}$$

where A is wings area, ρ is fluid density, b is wing span, $\bar{c}$ is average chord length, and the relationship between the coefficients and angles is

$$\begin{aligned}
C_D(\alpha) &= C_{D_0} + C_{D_\alpha}\alpha^2,\\
C_{SF}(\beta) &= C_{SF_\beta}\beta\\
C_L(\alpha) &= C_{L_\alpha}\alpha,\\
C_{T_1}(\beta) &= C_{T_{1\beta}}\beta\\
C_{T_2}(\alpha) &= C_{T_{2\alpha}}\alpha,\\
C_{T_3}(\beta) &= C_{T_{3\beta}}\beta.
\end{aligned} \qquad (6)$$

During testing, subtract the individual test data of the support bar from the measurements to eliminate the influence of the support bar. When measuring the pitching moment, the effects of the model and support bar weight on the torque can be eliminated by calibrating the balance zero drift. While measuring rolling and yawing moments, the effects of the sideslip force on the moments can be eliminated via the following:

$$M_s = M_0 - L_{SF}\times SF_b, \qquad (7)$$

where M_s is the moments after transfer, M_0 is the SRI measurements, L_{SF} is the distance between model gravity center and SRI, and SF_b is the projection of sideslip force in body coordinate system.

3. Numerical Modelling

The glider adopts ANSYS-FLUENT as its CFD computing software. The glider works within the range of low Reynolds numbers and the contrast is comparatively larger between the hull and wings. Select the RNG k-ε model and use the mode of double precision calculation with the model described below.

$$\rho\frac{Dk}{Dt} = \frac{\partial}{\partial x_i}\left[\left(\mu+\frac{\mu_t}{\sigma_k}\right)\frac{\partial k}{\partial x_i}\right] + G_k + G_b - \rho\varepsilon - Y_M, \qquad (8)$$

$$\begin{aligned}
\rho\frac{D\varepsilon}{Dt} &= \frac{\partial}{\partial x_i}\left[\left(\mu+\frac{\mu_t}{\sigma_k}\right)\frac{\partial \varepsilon}{\partial x_i}\right] + C_{1\varepsilon}\frac{\varepsilon}{k}\left(G_k + C_{3\varepsilon}G_b\right)\\
&\quad - C_{2\varepsilon}\rho\frac{\varepsilon^2}{k},
\end{aligned} \qquad (9)$$

where G_k is the product item of the turbulent kinetic energy, k caused by the average velocity gradient, G_b is the product item of the turbulent kinetic energy caused by buoyance, and Y_M is the effect of compressible turbulent fluctuation on the total dissipation rate. $\mu_t = \rho C_\mu k^2/\varepsilon$ is turbulent viscosity coefficient. In FLUENT calculation process, set $C_{1\varepsilon} = 1.44$, $C_{2\varepsilon} = 1.92$, $C_\mu = 0.09$, and the Turbulent Prandtl number of turbulent kinetic energy k and dissipation rate ε is $\sigma_k = 1.0$ and $\sigma_\varepsilon = 1.3$, respectively.

To reduce the impacts of the wall effects and simultaneously avoid excessive calculation, we restrict the water area to be a rectangle with length of 5Lglider width of 18Dglider wide, and height of 18Dglider, and set the distance between the glider buoyant center to the flow field inlet as 1.5Lglider, and let the length be 9Dglider, respectively, to the four walls (Left, Right, Upper, and Lower). The model meshing of the water area is shown in Figure 4.

4. Results and Discussion

4.1. Hydrodynamic Coefficient Measurements. According to (4) and (5), the force and moment coefficients can be obtained.

In the case of Configuration 1, the relationship can be obtained between the attack angles and the glider lift, drag, and pitching moment coefficients as shown in Figure 5.

The relationship can be obtained between the drift angles and the glider sideslip force, rolling moment, and yawing moment coefficients as shown in Figure 6.

As shown in Figures 5 and 6, the data obtained in such a low-speed condition as 0.15m/s (2.0m/s wind speed) will suffer from a comparatively violent fluctuation due to the wind

speed and measurements being unstable in low-speed conditions. In a high-speed condition as 12m/s, it can be observed that the wings are jittering, but stable data can be obtained after filter processing. The curves of the coefficients obtained in the case of different velocities are comparatively close to each other and it may also be applicable to the parameters in cases of a high-speed condition.

As shown in Figure 6(b), the rolling moment coefficient obtained features poor consistency primarily due to the modes of the SRI installation. During testing, what the balance has measured is the rolling moment relative to the lower pivot. A conversion should be made according to (7). The subtraction process will overlay errors and have deviations that exist in estimation of the force arm state, thus causing significant errors after the data has been converted.

As shown in Figures 5(c) and 6(c), the pitching and yawing moments have formed a positive feedback to the angles. Specifically, when an attack or sideslip angle has been formed, the moment will tend to have the angle become greater, thus causing the glider instability. It can be seen that the longitudinal and rotational motions of the designed glider both lack hydrodynamic stability.

4.2. Comparison of Experimental and Numerical Results. To calibrate the results of the numerical calculation, compare the measurements with the average values of the 6 hydrodynamic coefficients calculated from the two kinds of gliders at their conventional speed (0.25m/s and 0.35m/s). Use the least square method for data fitting and the force and moment coefficients relative to the angles, as shown in Figure 7, will be obtained; See Table 4 for the errors between the numerical calculation values and the measured values.

As shown in Figure 7 and Table 4, some differences exist between the measurements and the numerical values because the wind tunnel test is more complicated and has more complex boundary separation situations.

As shown in Figure 7(e) and Table 4, the drag coefficient has its measurements greater than the numerical value which is mainly characterized by the larger difference of the quadratic function deviation coefficient C_{D_0}. The difference occurs because the numerical calculation uses an ideal model, without considering the drag produced from such factors as the surface roughness, wing deformation, and small protrusions, etc.

As shown in Figures 7(e) and 7(f) and Table 4, the rolling and yawing moment coefficients are numerically small. If there is a nonzero sideslip angle, the rolling and yawing restoring moments will be small. In the presence of a disturbance, the glider may have a longer vibration period.

4.3. Impacts of Hydrodynamic Coefficient on Glider Movement. To verify the impacts of the hydrodynamic coefficients on the glider movement performance, use the two groups of hydrodynamic coefficient results obtained in the previous section in order to carry out the gliding path of the glider. To analyze the hydrodynamic impacts on the movement, use a simplified glider model for analysis and the control variables of the simplified model including the following two parts: the buoyancy subject to a fixed position and a variable mass and the sliding block subject to a fixed mass and a variable position. See Figure 8 for the simplified model, with the corresponding parameters as described in Table 5. See Zhang et al. [8] for definitions of the model parameters. See Appendix A for the dynamical model, and see Appendix B for parameters of the designed glider.

Table 4: Comparison of CFD results and measurements.

coefficient	Exp.	CFD	%Dev
C_{D_0}	0.1185	0.09209	22.29
C_{D_α}	0.001614	0.001555	3.66
C_{L_α}	0.1066	0.09448	11.37
$C_{T_{2\alpha}}$	0.04835	0.04165	13.86
C_{SF_β}	-0.01601	-0.01378	13.93
$C_{T_{1\beta}}$	-0.0006173	-0.0003491	43.45
$C_{T_{3\beta}}$	-0.002873	-0.003359	-16.92

Carry out the simulation analysis of the hydrodynamic parameter impacts on the 2D motion paths of the glider. Use the two sets of hydrodynamic parameters given in Table 4, respectively, to obtain the motion paths. Assume the glider starts from the depth of 0 meters, glides downward to the depth of 300 meters, and then glides back to the depth of 0 meters. During downward and upward transformation, the (r_{px}, m_b) status changes from (0.015m, 1.3kg) to (-0.015m, 0.7kg). To obtain the movement paths, the glide angle, the glide velocity, and the turning radius are needed. To solve the steady-state solution of the equations in Appendix A, the left side of the equals sign is set to zero. Obtain the solutions by Least Square Form of Evaluation Function.

$$F = f_1^2 + f_2^2 + f_3^2 + f_4^2 + f_5^2 + f_6^2, \tag{10}$$

When $F \longrightarrow 0$, the solution of the system is obtained. The PSO algorithm is used to obtain the parameters of dynamic equations when $F \longrightarrow 0$. PSO algorithm randomly selects the initial particle point and keeps iterating until the convergent region is reached. The general equation of PSO is

$$\begin{aligned} v_i(t+1) = {} & v_i(t) + c_1 r_1 \left(p_i - x_i(t)\right) \\ & + c_2 r_2 \left(g_i - x_i(t)\right), \end{aligned} \tag{11}$$

$$x_i(t+1) = x_i(t) + v_i(t+1), \tag{12}$$

where v_i is the speed of particle i, x_i is the position of particle i, c_1, c_2 are the acceleration parameters, r_1, r_2 are the random number between 0 and 1, p_i is the last optimal position of particle i, and g_i is the global optimal position.

See Figure 9(a) for the moving path of a gliding cycle.

Set a clockwise 20° rotation angle of the sliding block based on the 2D motion settings so that the turning spiral path can be obtained as shown in Figure 9(b).

The hydrodynamic force will affect the balance of the glider force and moment, as well as consequently affecting the steady gliding path. As shown in Table 5, the drag coefficient subject to the CFD is smaller than the measurements and thus results in a higher speed and a smaller gliding angle so that the

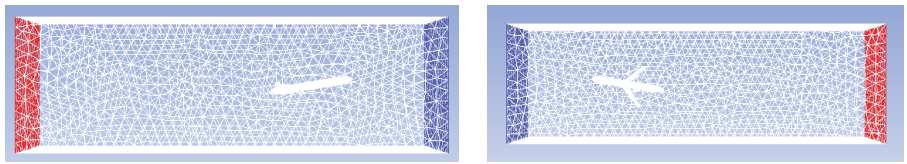

(a) Pitching configuration (b) Turning configuration

Figure 4: The model meshing of water area.

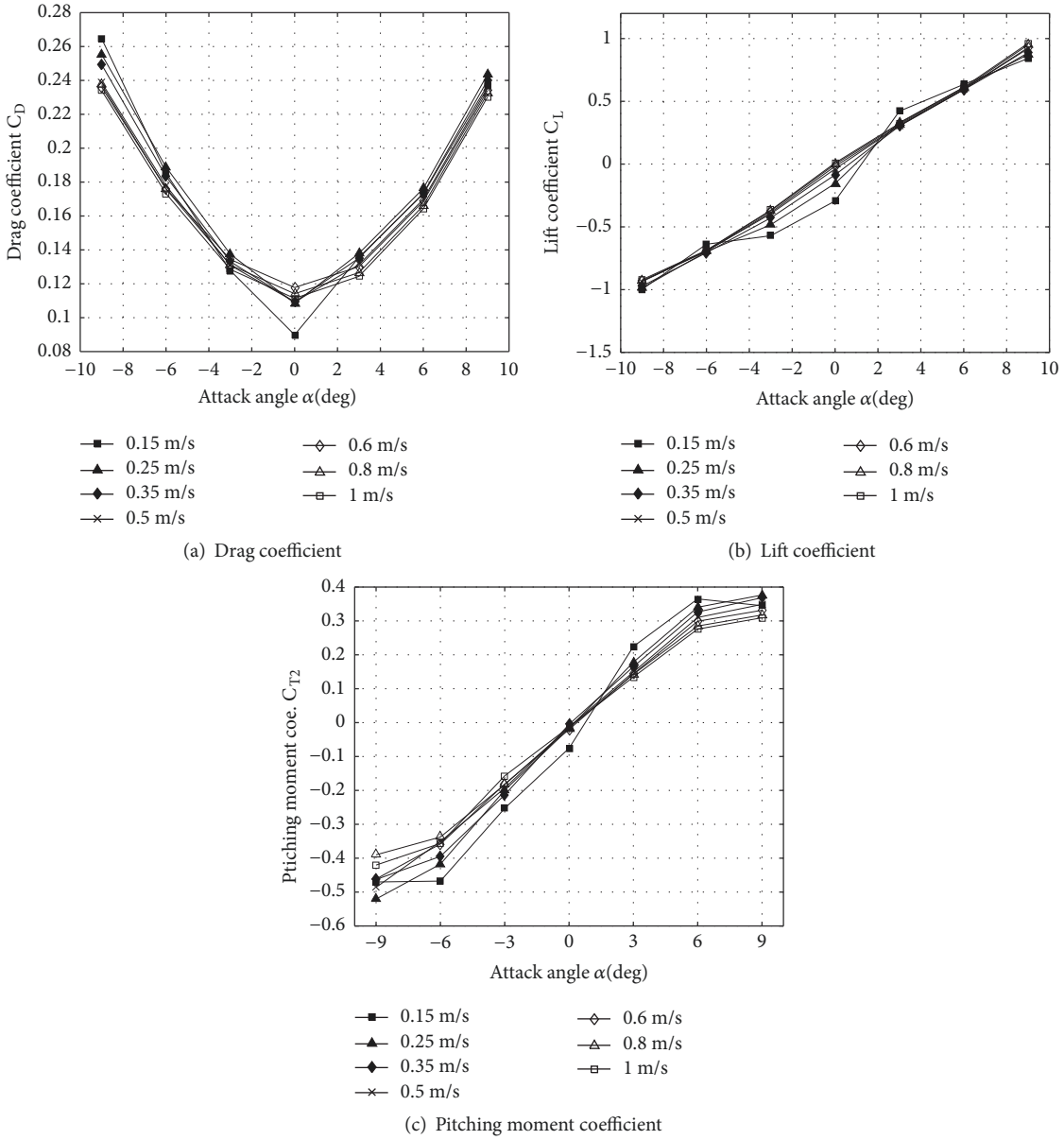

(a) Drag coefficient (b) Lift coefficient

(c) Pitching moment coefficient

Figure 5: Hydrodynamic force and moment coefficients in wing-level state.

running distance will be longer under the same conditions. Compared with the moment produced by the glider body, the hydrodynamic moment is comparatively small but still has some influences on the moment balance. The pitching moment coefficient subject to the CFD result is smaller than the measurements and thus results in a smaller gliding angle while the yawing moment coefficient is larger than the measured value resulting in a larger turning radius. Due to the differences that exist between the paths generated via the CFD results and measurements, as shown in Figure 8, when

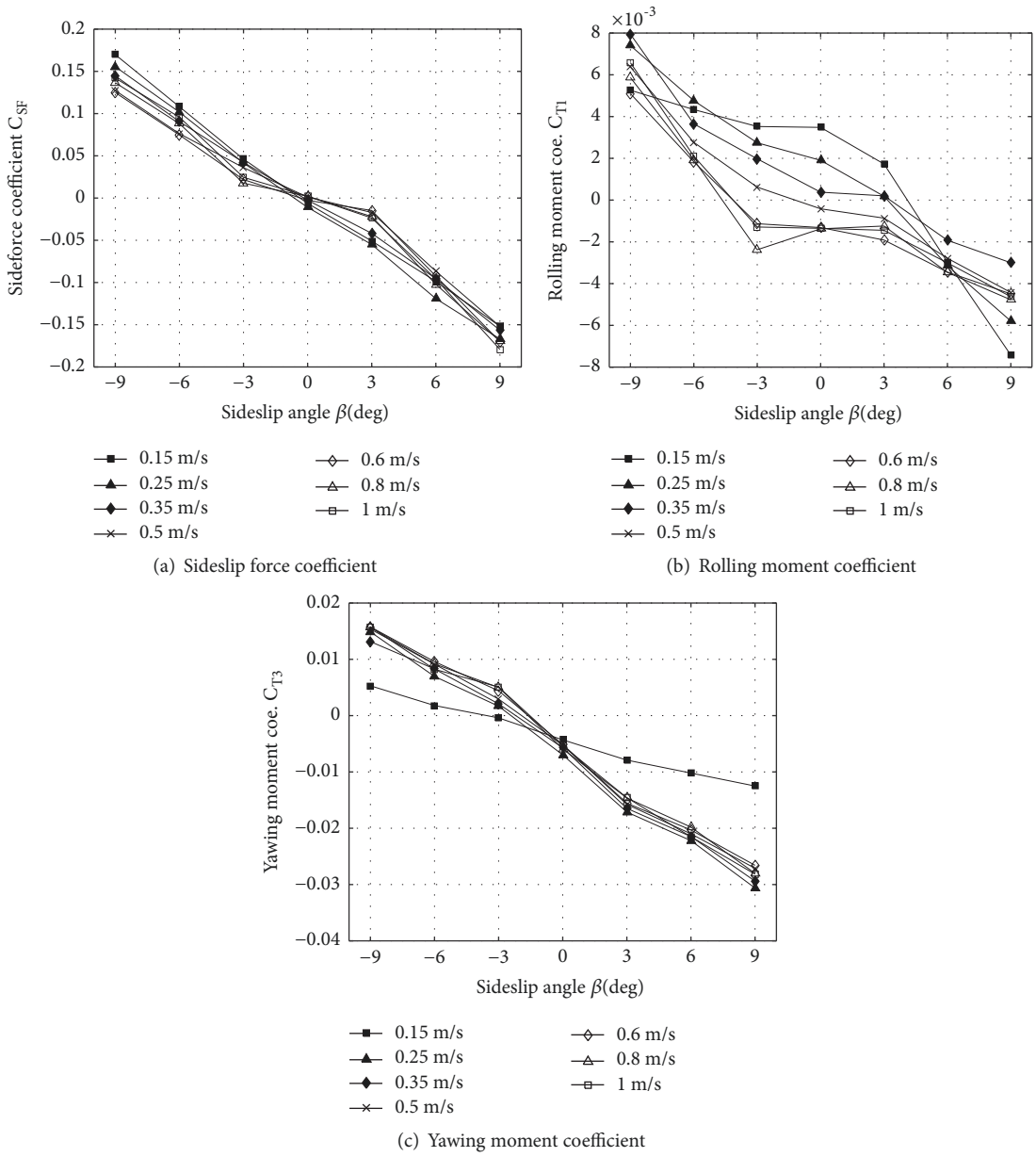

Figure 6: Hydrodynamic force and moment coefficients in spiraling state.

the glider gliding near in a typical 30 degrees, the error of 2D trajectory is 2.5% percent subject to the horizontal distance in 1000m range under two sets of hydrodynamic parameters. Since the glider has a large working area, the error of about 2.5% will not have a significant impact on the trajectory and the results from the CFD can basically reflect the state of the gliding path. For the turning case, when the turning radius is around 10m, the radius error is about 12.45%, which resulted mainly from deviations of rolling moment coefficients. As shown in f_4, f_5, and f_6 of dynamic equation in Appendix, when the angle of attack and the angle of drift are small, the rolling moment, the pitching moment, and the yawing moment will all have a great impact on the equilibrium equation, among which the rolling moment value is bigger than the other two coefficients. Moreover, the large deviation of rolling moment between the experimental result and the numerical result indicates that the turning radius error mainly comes from the error of rolling moment coefficients.

4.4. Estimation of Drag Coefficient. The drag coefficient is an important parameter in the design process of gliders because it directly influences the velocity of gliders. In order to simplify the design process of gliders, we fit the empirical formula based on the experimental data. The research of Sherman et al. [4] and Jagadeesh et al. [10] shows that the drag coefficient is related not only to the attack angle but also to the Reynolds number. The Reynolds number contains the velocity parameter of motion, and if the Reynolds number is removed from the drag coefficient, the obtained parameters

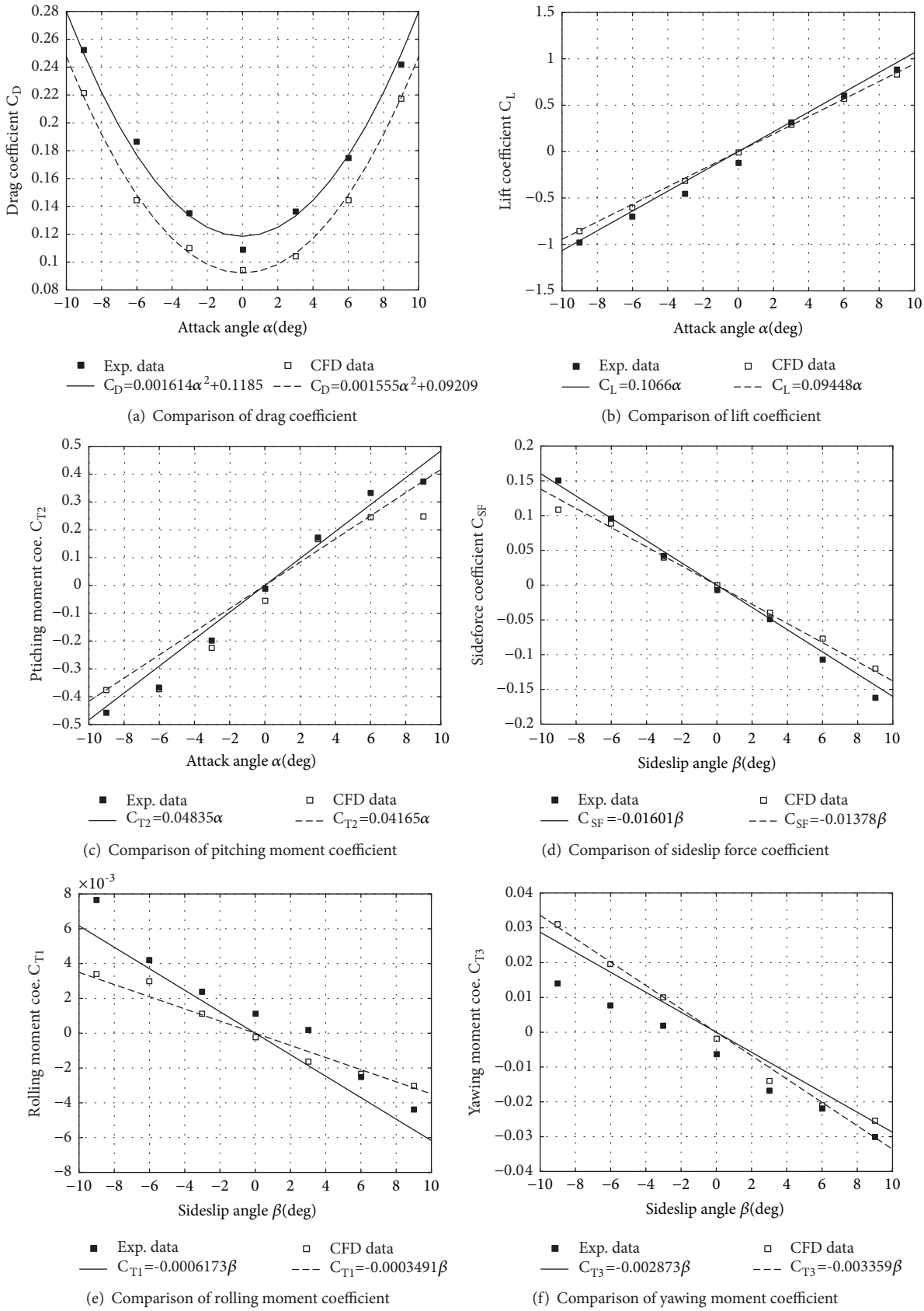

(a) Comparison of drag coefficient

(b) Comparison of lift coefficient

(c) Comparison of pitching moment coefficient

(d) Comparison of sideslip force coefficient

(e) Comparison of rolling moment coefficient

(f) Comparison of yawing moment coefficient

Figure 7: Comparison between CFD results and measurements in Configuration 1.

Table 5: Path states under different hydrodynamic parameters.

Movement mode	States	Hydrodynamic parameters	Gliding angle (°)	Velocity (m/s)	Turning radius (m)
2D	Downward	Experiment	-31.6621	0.3881	0
		CFD	-30.9861	0.4360	0
	Upward	Experiment	31.6621	0.3881	0
		CFD	30.9861	0.4360	0
3D	Downward	Experiment	-33.1626	0.4084	10.2590
		CFD	-31.0574	0.4432	11.7181

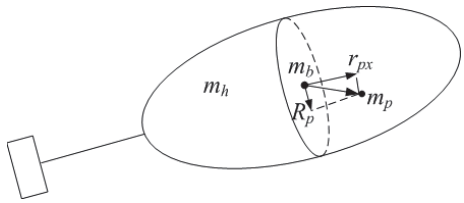

Figure 8: Simplified underwater model.

will be more applicable. We give the explicit expression of Reynold number in the drag coefficient as in the following:

$$C_D = \left(a + b \cdot \alpha^2\right)\left(R_e^{-1/8}\right), \tag{13}$$

To obtain the coefficients a and b, we collect a set of values α_i, R_{e_i}, and C_{D_i}, where $i = 1, ..., n$, and solve the following nonlinear system:

$$0 = \left(a + b \cdot {\alpha_i}^2\right)\left(R_{e_i}^{-1/8}\right) - C_{D_i}, \tag{14}$$

The Matlab function fsolve is used to the above nonlinear system, obtaining $a = 0.67$ and $b = 0.0085$. The fitted curve of drag coefficient is given by Figure 10.

In order to verify the applicability of the formula, we select the frontal cross area of the body as the characteristic area, which is 0.0356, following Williams et al. [14] and Graver [17]. We obtained $C_{d0} = 0.3278$, $C_{d\alpha} = 13.68$, while $C_{d0} = 0.214$ and $C_{d\alpha} = 32.3$ are given in Graver et al. [13], and $C_{d0} = 0.246$ and $C_{d\alpha} = 6.18$ are given Williams et al. [14], respectively. We can see that the value obtained by our method falls in the middle of the other two sets. The subtle differences may be caused by the different configurations and the different running environments.

4.5. Impact of Appendage on Drag. Test the impacts of the appendages on the glider drag at different velocities based on the set of a 0° attack angle and 0° sideslip angle. See Figures 11 and 12, respectively, for the impacts of the CTD unit and propeller on the glider drag.

As shown in Figure 11(a), the glider drag measurements are relatively close to each other and numerically small in the presence and absence of the CTD. Four groups of measurements that are less than 1% of the SRI measurement range (0.7 N). In order to eliminate the impacts of the measurement errors, select three groups of data with measurements greater than 0.7 N for analysis. Compare the drag values in Configuration 1 and Configuration 2 to find that the maximum and average differences are 2.70% and 2.38%, respectively. The CTD surface area accounts for approximately 1.1% of the glider total area and, thus, when the glider is carrying a CTD unit, the drag increase is mainly caused by the CTD frictional drag. This result is significantly different from the conclusion of an approximate difference of 40% which was given by Graver et al. [13] and Techy et al. [16]. The possible reasons may be as follows: the CTD units they used is of an irregular shape and thus produce form drag, while the CTD units used in this test are streamlined and thus produce smaller drag. As shown in Figure 11(b), the average error between the two sets is 0.0038, and the deviation is about 3.2% subject to C_{D_0}, which is relatively small, and have less impact on the movement of the glider.

As shown in Figure 12(a), closed drags can be obtained under two mounting configurations of propeller. If the propeller is mounted outside, the drag of the glider will be increased by approximately 1% max. If the propeller is mounted inside, the drag of the glider will be decreased by 1.5% instead. The reasons for this phenomenon is not yet clear, but there are three potential factors:

(1) The force measured in two cases suffers from the maximum difference of 0.0518 N which is 1% less than the SRI measurement range (0.7N), so the difference has resulted from the measurement error of the balance.

(2) For built-in propeller testing regarding condition, there is a diversion hole that opens on the tail water deflector where the missing part has reduced the hull surface and thus lowered the surface frictional drag.

(3) The external (Configuration 4) mounting mode of the propeller causes the complex change of the fluid in the tail of the hull, and the tail vortex is generated to form a positive pressure.

As shown in Figure 12(b), in the low-speed region, the deviation among the three sets data are disorderly. In the high-speed region, the difference among them is clearer, but the same as the CTD mounting status, the difference between the different mounting method of propeller will have less impact on the movement of the glider.

In conclusion, the above analysis shows that the mounting modes of propeller will have a minor impact on glider drag when mounted.

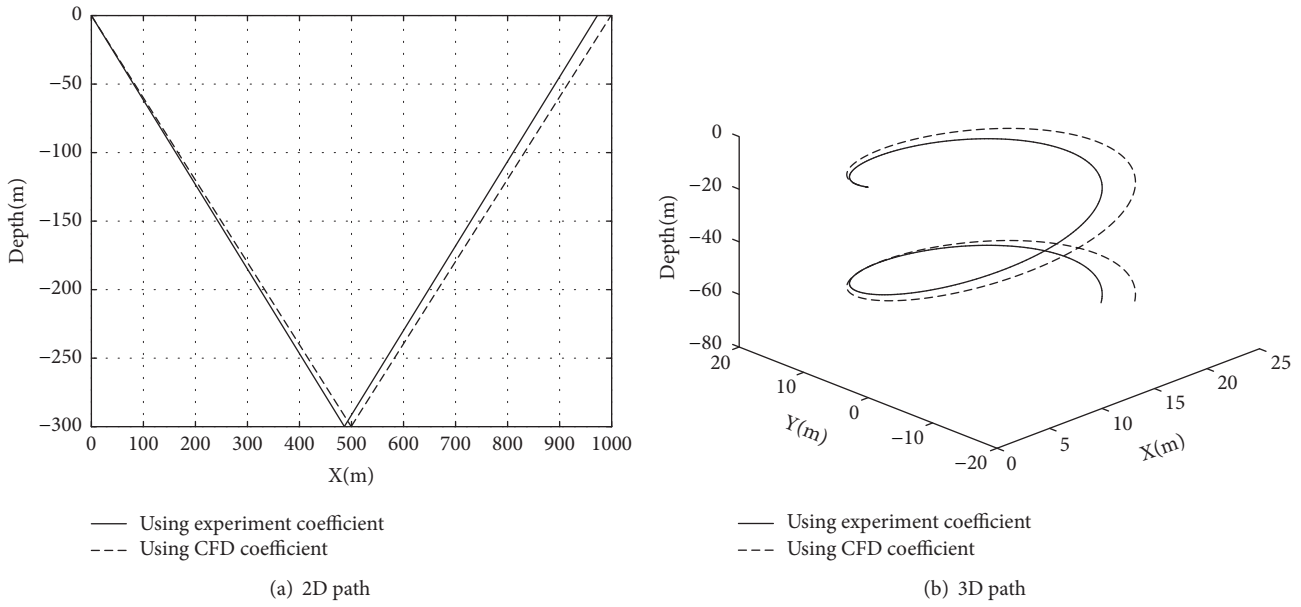

(a) 2D path (b) 3D path

Figure 9: Comparison of path under different hydrodynamic coefficients.

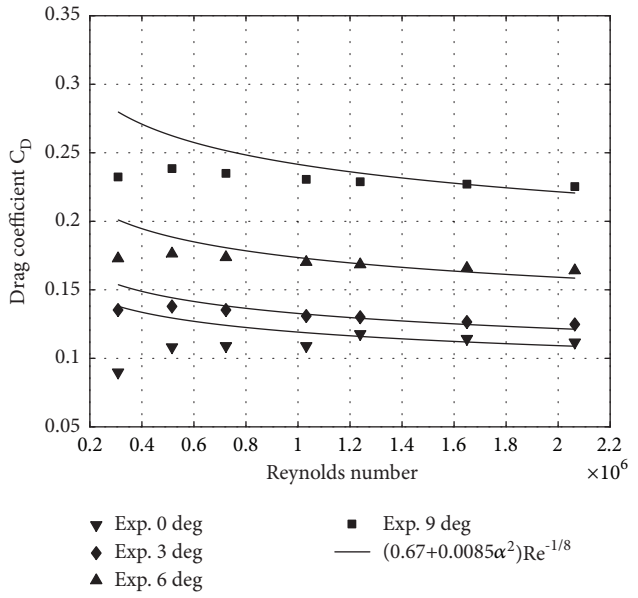

Figure 10: The drag coefficient curve with Reynolds number.

5. Conclusions

In order to obtain the correct hydrodynamic parameters of underwater glider, in this paper, firstly, a wind tunnel experiment is configured based on the Reynolds number similarity criterion, equivalently converts underwater movement into air, and determines the corresponding testing wind speed; secondly, hydrodynamic coefficients are obtained from measured and numerical data, respectively, by using fitting method and combined with hydrodynamic parametric equation; thirdly, based on the dynamic equation, the paths generated by two sets of parameters obtained from measured and numerical calculations are compared, where a PSO numerical algorithm is used to solve the 6-DOF steady-state equation. The difference between the two groups of parameters is reflected by the difference of movement path. Besides, the experimental data provide a modification guidance and a referential basis to numerical calculated results; fourthly, the empirical formula of drag coefficient with Reynolds number is obtained based on the experimental data, and the formula

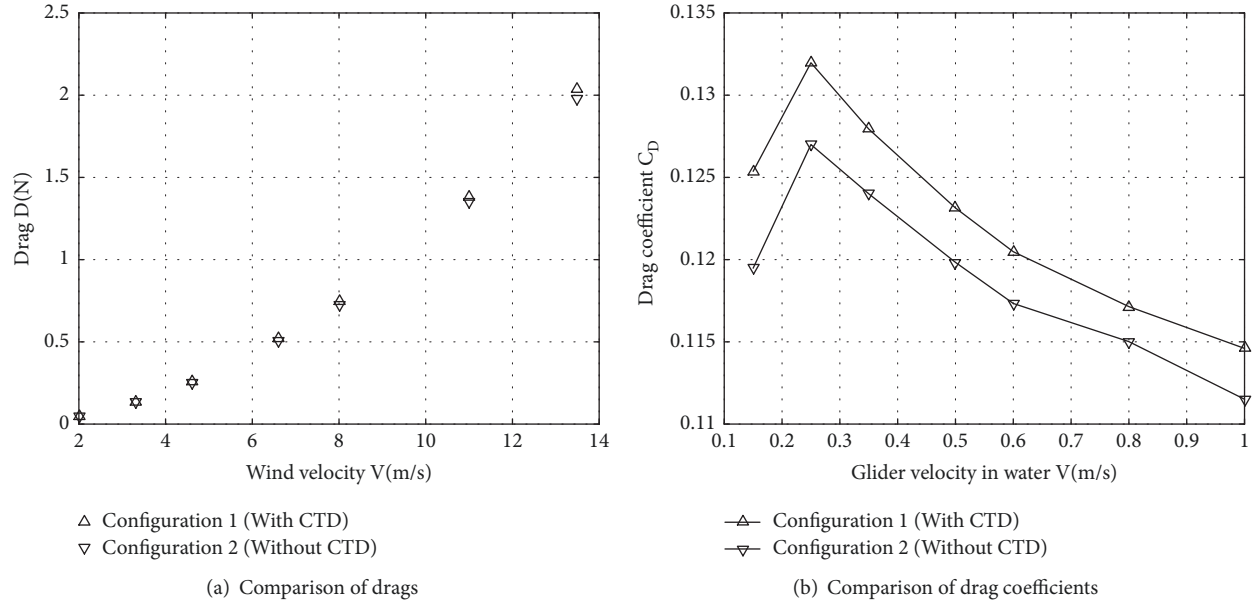

(a) Comparison of drags

(b) Comparison of drag coefficients

Figure 11: Comparison of glider drags with and without CTD.

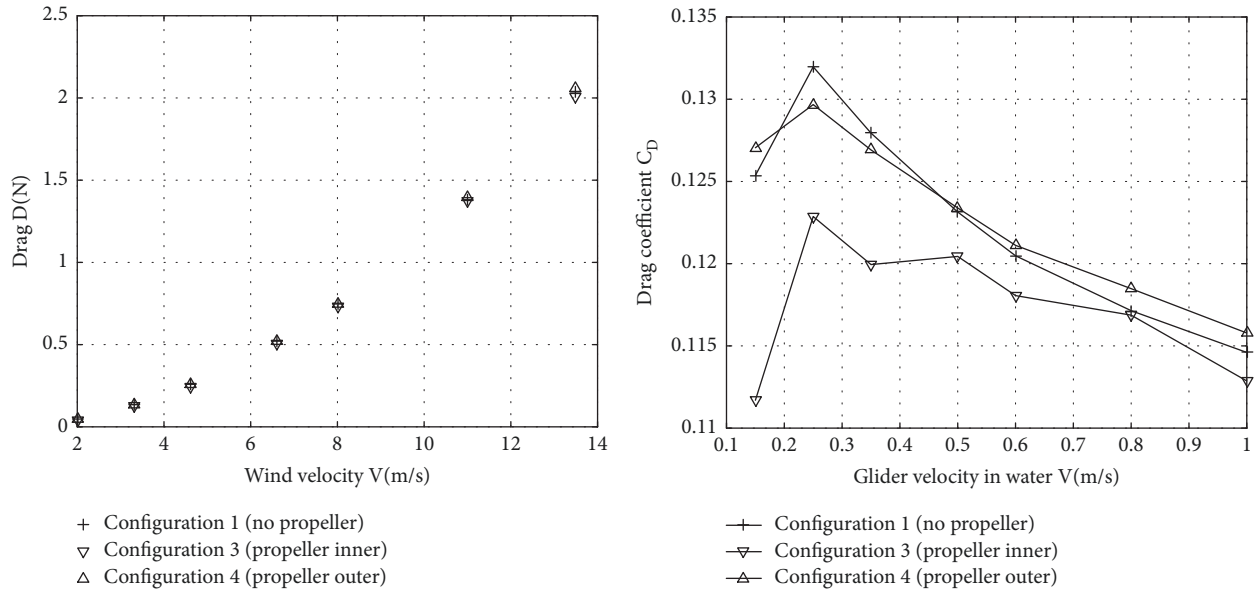

(a) Comparison of drags

(b) Comparison of drag coefficients

Figure 12: Comparison of glider drags in different propeller configuration.

can be used for the simple design of the glider; and finally, the change of the body drag caused by the appendage is studied.

The main conclusions are as follows.

(1) The rolling and yawing moment coefficients are numerically small, which indicates that when there is a nonzero sideslip, the rolling and yawing restoring moment are small. The body may have a longer swing period in the presence of external interference.

(2) The comparison between the numerical results and the measurements shows that the 2D path error caused by the two parameters is about 2.5%, and the hydrodynamic coefficients obtained by $RNGk - \varepsilon$ method can be used for glider design and the movement analysis.

(3) The drag of glider with CTD is bigger than that without it. When the CTD is streamline shape, the increased drag is generated by frictional drag. In order

to decrease body drag, the carried appendages should be streamline shape.

(4) According to experimental results, the two modes of carrying appendages, inside or outside, have little influence on body drag.

Appendix

A. Dynamics Model

The 6-DOF Steady-State Gliding Dynamic Equation of Underwater Glider.

$$
\begin{aligned}
f_1 &= L\sin\alpha - SF\cos\alpha\sin\beta - D\cos\alpha\cos\beta \\
&\quad - m_0 g\sin\theta + \dot{\psi}\cos\theta\left[\left(m_p + m_2\right)v_2\cos\varphi\right. \\
&\quad \left. - \left(m_p + m_3\right)v_3\sin\varphi\right] + m_p\dot{\psi}^2\left[r_{p_x}\cos^2\theta\right. \\
&\quad \left. + \frac{\mathrm{R}_p\cos\left(\varphi+\mu\right)\sin 2\theta}{2}\right] \\
f_2 &= SF\cos\beta - D\sin\beta + m_0 g\sin\varphi\cos\theta \\
&\quad - \dot{\psi}\left[\left(m_p + m_3\right)v_3\sin\theta\right. \\
&\quad \left. + \left(m_p + m_1\right)v_1\cos\varphi\cos\theta\right] \\
&\quad - m_p\dot{\psi}^2\left[\frac{1}{2}\mathrm{R}_p\cos\mu\cos^2\theta\sin 2\varphi\right. \\
&\quad \left. + \mathrm{R}_p\sin\mu\left(1-\sin^2\varphi\cos^2\theta\right) - \frac{1}{2}r_{p_x}\sin 2\theta\sin\varphi\right] \\
f_3 &= -L\cos\alpha - SF\sin\alpha\sin\beta - D\sin\alpha\cos\beta \\
&\quad + m_0 g\cos\varphi\cos\theta + \dot{\psi}\left[\left(m_p + m_2\right)v_2\sin\theta\right. \\
&\quad \left. + \left(m_p + m_1\right)v_1\sin\varphi\cos\theta\right] \\
&\quad + m_p\dot{\psi}^2\left[\frac{1}{2}r_{p_x}\sin 2\theta\cos\varphi\right. \\
&\quad + \frac{1}{2}\mathrm{R}_p\cos^2\theta\sin 2\varphi\sin\mu \\
&\quad \left. + \mathrm{R}_p\cos\mu\left(1-\cos^2\theta\cos^2\varphi\right)\right] \\
f_4 &= MDL_1\cos\alpha\cos\beta - MDL_2\cos\alpha\sin\beta \\
&\quad - MDL_3\sin\alpha - m_p g\mathrm{R}_p\cos\theta\ \sin\left(\mu+\varphi\right) \\
&\quad + v_2 v_3\left(m_2 - m_3\right) + \mathrm{R}_p\dot{\psi}m_p\sin\theta\left(v_3\cos\mu\right. \\
&\quad \left. - v_2\sin\mu\right) + \mathrm{R}_p\dot{\psi}m_p v_1\cos\theta\ \cos\left(\mu+\varphi\right) + \frac{1}{2} \\
&\quad \cdot \mathrm{R}_p{}^2\dot{\psi}^2 m_p\cos^2\theta\sin 2\left(\mu+\varphi\right) + \frac{1}{2} \\
&\quad \cdot \dot{\psi}^2\cos^2\theta\sin 2\varphi\left(J_2 - J_3\right) - \frac{1}{2} \\
&\quad \cdot \mathrm{R}_p r_{p_x}\dot{\psi}^2 m_p\sin 2\theta\ \sin\left(\mu+\varphi\right) \\
f_5 &= MDL_2\cos\beta + MDL_1\sin\beta \\
&\quad - m_p g\left(\mathrm{R}_p\cos\mu\sin\theta + \cos\varphi\cos\theta r_{p_x}\right) \\
&\quad - v_3\mathrm{R}_p\dot{\psi}m_p\cos\theta\ \sin\left(\mu+\varphi\right) + v_1 v_3\left(m_3 - m_1\right) \\
&\quad - v_1\dot{\psi}r_{p_x}m_p\sin\varphi\cos\theta - v_2\dot{\psi}r_{p_x}m_p\sin\theta - \frac{1}{2} \\
&\quad \cdot \mathrm{R}_p{}^2\dot{\psi}^2 m_p\ \sin\left(\mu+\varphi\right)\sin 2\theta\sin\mu \\
&\quad - \mathrm{R}_p\dot{\psi}^2 r_{p_x}m_p\sin^2\theta\cos\mu - \frac{1}{2} \\
&\quad \cdot \dot{\psi}^2 r_{p_x}{}^2 m_p\cos\varphi\sin 2\theta \\
&\quad + \mathrm{R}_p\dot{\psi}m_p\cos\varphi\cos\theta\left(v_2\cos\mu + v_3\sin\mu\right) \\
&\quad + \mathrm{R}_p\dot{\psi}^2 r_{p_x}m_p\cos^2\theta\ \cos\left(\mu+\varphi\right)\cos\varphi + \frac{1}{2} \\
&\quad \cdot \mathrm{R}_p{}^2\dot{\psi}^2 m_p\sin 2\theta\cos\varphi + \frac{1}{2}\dot{\psi}^2\sin 2\theta\cos\varphi\left(J_1\right. \\
&\quad \left. - J_3\right) \\
f_6 &= MDL_1\sin\alpha\cos\beta - MDL_2\sin\alpha\sin\beta \\
&\quad + MDL_3\cos\alpha + m_p g\left(\cos\theta\sin\varphi r_{p_x}\right. \\
&\quad \left. - \mathrm{R}_p\sin\mu\sin\theta\right) + v_2\mathrm{R}_p\dot{\psi}m_p\cos\theta\ \sin\left(\mu+\varphi\right) \\
&\quad + v_1 v_2\left(m_1 - m_2\right) - v_1 r_{p_x}\dot{\psi}m_p\cos\theta\cos\varphi \\
&\quad - v_3 r_{p_x}\dot{\psi}m_p\sin\theta - \mathrm{R}_p r_{p_x}\dot{\psi}^2 m_p\sin^2\theta\sin\mu + \frac{1}{2} \\
&\quad \cdot r_{p_x}{}^2\dot{\psi}^2 m_p\sin 2\theta\sin\varphi + \frac{1}{2}\mathrm{R}_p{}^2\dot{\psi}^2 m_p\ \sin\left(\mu+\varphi\right)\sin 2\theta\cos\mu \\
&\quad - \mathrm{R}_p r_{p_x}\dot{\psi}^2 m_p\cos^2\theta\ \cos\left(\mu+\varphi\right)\sin\varphi - \frac{1}{2} \\
&\quad \cdot \mathrm{R}_p{}^2\dot{\psi}^2 m_p\sin 2\theta\sin\varphi \\
&\quad - \mathrm{R}_p\dot{\psi}m_p\sin\varphi\cos\theta\left(v_3\sin\mu + v_2\cos\mu\right) + \frac{1}{2} \\
&\quad \cdot \dot{\psi}^2\sin 2\theta\sin\varphi\left(J_2 - J_1\right)
\end{aligned}
\tag{A.1}
$$

The meaning of each parameter is shown in Table 6.

B. The Characteristic Parameters of the Designed Underwater Glider

See Table 7.

Data Availability

The data used to support the findings of this study are available from the corresponding author upon request.

Conflicts of Interest

The authors declare that there are no conflicts of interest regarding the publication of this paper.

Table 6: Meaning of parameters.

Parameters	Physical Significance
$[MDL_1, MDL_2, MDL_3]$	Roll, Pitch and Yaw moment
$[L, D, SF]$	Lift, Drag and Lateral force
$[m_1, m_2, m_3]$	Additional mass
$[J_1, J_2, J_3]$	Additional inertial mass
$[\alpha, \beta]$	Angle of attack and slide
m_p	Mass of slider
$[v_1, v_2, v_3]$	Velocity components in body coordinates
$[R_p, r_{p_x}]$	Radial and Axial Position of Sliding Mass Center in the body coordinates
θ	Pitch angle
μ	Slider angle
φ	Roll angle
$\dot{\psi}$	Yawing rate

Table 7: Values of parameters.

Parameter meaning	Values
Glider total mass m (kg)	65
Glider uniform mass m_h (kg)	51
Slider block mass m_p (kg)	13
Buoyancy mass m_b (kg)	1±0.5
Slider block position in x axis r_{px} (m)	±0.05
Slider block position in z axis R_p (m)	0.02
Added mass of hull $[m_{f1}, m_{f2}, m_{f3}]$ kg	[2, 50, 60]
Added inertia of hull $[J_{f1}, J_{f2}, J_{f3}]$ kg.m^2	[0.2, 8, 10]

Acknowledgments

This work was supported by the NSFC Projects of China under Grant no. 61403250.

References

[1] D. L. Rudnick, K. D. Zaba, R. E. Todd, and R. E. Davis, "A climatology of the California Current System from a network of underwater gliders," *Progress in Oceanography*, vol. 154, pp. 64–106, 2017.

[2] D. C. Webb, P. J. Simonetti, and C. P. Jones, "SLOCUM: An underwater glider propelled by environmental energy," *IEEE Journal of Oceanic Engineering*, vol. 26, no. 4, pp. 447–452, 2001.

[3] C. C. Eriksen, T. J. Osse, R. D. Light et al., "Seaglider: A long-range autonomous underwater vehicle for oceanographic research," *IEEE Journal of Oceanic Engineering*, vol. 26, no. 4, pp. 424–436, 2001.

[4] J. Sherman, R. E. Davis, W. B. Owens, and J. Valdes, "The autonomous underwater glider "Spray"," *IEEE Journal of Oceanic Engineering*, vol. 26, no. 4, pp. 437–446, 2001.

[5] M. Y. Javaid, M. Ovinis, F. B. M. Hashim, A. Maimun, Y. M. Ahmed, and B. Ullah, "Effect of wing form on the hydrodynamic characteristics and dynamic stability of an underwater glider," *International Journal of Naval Architecture and Ocean Engineering*, vol. 9, no. 4, pp. 382–389, 2016.

[6] C. Sun, B. Song, and P. Wang, "Parametric geometric model and shape optimization of an underwater glider with blended-wing-body," *International Journal of Naval Architecture and Ocean Engineering*, vol. 7, no. 6, pp. 995–1006, 2015.

[7] J. S. Geisbert, *Hydrodynamic modeling for autonomous underwater vehicles using computational and semi-empirical methods [MSc thesis]*, Virginia Polytechnic Institute and State University, 2007.

[8] S. Zhang, J. Yu, A. Zhang, and F. Zhang, "Spiraling motion of underwater gliders: Modeling, analysis, and experimental results," *Ocean Engineering*, vol. 60, pp. 1–13, 2013.

[9] K. Isa, M. R. Arshad, and S. Ishak, "A hybrid-driven underwater glider model, hydrodynamics estimation, and an analysis of the motion control," *Ocean Engineering*, vol. 81, pp. 111–129, 2014.

[10] P. Jagadeesh, K. Murali, and V. G. Idichandy, "Experimental investigation of hydrodynamic force coefficients over AUV hull form," *Ocean Engineering*, vol. 36, no. 1, pp. 113–118, 2009.

[11] B. J. Guo, G. B. Deng, and S. Steen, "Verification and validation of numerical calculation of ship resistance and flow field of a large tanker," *Ships and Offshore Structures*, vol. 8, no. 1, pp. 3–14, 2013.

[12] M. Nakamura, K. Asakawa, T. Hyakudome, S. Kishima, H. Matsuoka, and T. Minami, "Hydrodynamic coefficients and motion simulations of underwater glider for virtual mooring," *IEEE Journal of Oceanic Engineering*, vol. 38, no. 3, pp. 581–597, 2013.

[13] G. J. Graver, R. Bachmayer, E. N. Leonard et al., "Underwater glider model parameter identification," in *Proceedings of the 13th International Symposium on Unmanned Untethered Submersible Technology (UUST)*, vol. 1, pp. 12-13, 2003.

[14] C. D. Williams, R. Bachmayer, and B. deYoung, "Progress in predicting the performance of ocean gliders from at-sea measurements," in *Proceedings of the OCEANS 2008*, pp. 1–8, Quebec City, QC, Canada, September 2008.

[15] S. Berman, *Comparison of the lift, drag and pitch moment coefficients of a Slocum glider wind tunnel model with computational results by Vehicle Control Technologies*, Princeton Univ., Princeton, NJ, MAE, 222.

[16] L. Techy, R. Tomokiyo, and J. Quenzer, "Full-scale wind tunnel study of the seaglider underwater glider," Tech. Rep., University of Washington, Aeronautics & Astronautics, Seattle, 2010.

[17] J. G. Graver, *Underwater gliders: Dynamics, control and design [PhD thesis]*, Princeton University, 2005.

[18] C. Yang, S. Peng, S. Fan, S. Zhang, P. Wang, and Y. Chen, "Study on docking guidance algorithm for hybrid underwater glider in currents," *Ocean Engineering*, vol. 125, pp. 170–181, 2016.

[19] W.-D. Niu, S.-X. Wang, Y.-H. Wang, Y. Song, and Y.-Q. Zhu, "Stability analysis of hybrid-driven underwater glider," *China Ocean Engineering*, vol. 31, no. 5, pp. 528–538, 2017.

[20] Z. Chen, J. Yu, A. Zhang, and F. Zhang, "Design and analysis of folding propulsion mechanism for hybrid-driven underwater gliders," *Ocean Engineering*, vol. 119, pp. 125–134, 2016.

[21] F. Liu, Y. Wang, W. Niu, Z. Ma, and Y. Liu, "Hydrodynamic performance analysis and experiments of a hybrid underwater glider with different layout of wings," in *Proceedings of the OCEANS 2014 MTS/IEEE Taipei Conference: Oceans Regeneration*, twn, April 2014.

[22] N. Mahmoudian, *Efficient motion planning and control for underwater gliders [PhD thesis]*, Virginia Polytechnic Institute and State University, 2009.